Direct evidence of Be as an amphoteric dopant in GaN

U. Wahl,[1,*] J. G. Correia,[1] A. R. G. Costa,[2] T. A. L. Lima,[2] J. Moens,[2] M. J. Kappers,[3] M. R. da Silva,[4] L. M. C. Pereira,[2] and A. Vantomme[2]

[1]*Centro de Ciências e Tecnologias Nucleares, Departamento de Engenharia e Ciências Nucleares, Instituto Superior Técnico, Universidade de Lisboa, 2695-066 Bobadela LRS, Portugal*

[2]*KU Leuven, Quantum Solid-State Physics, 3001 Leuven, Belgium*

[3]*Cambridge Centre for Gallium Nitride, University of Cambridge, Cambridge CB3 0FS, United Kingdom*

[4]*CICECO, Institute of Materials, Universidade de Aveiro, 13810-193 Aveiro, Portugal*

(Received 24 January 2022; accepted 13 May 2022; published 27 May 2022)

The interest in Be as an impurity in GaN stems from the challenge to understand why GaN can be doped *p* type with Mg, while this does not work for Be. While theory has actually predicted an acceptor level for Be that is shallower than Mg, it was also argued that Be is not a suitable acceptor because its amphoteric nature, i.e., its tendency to occupy substitutional Ga as well as interstitial sites, would be considerably more pronounced than for Mg and hence lead to self-compensation. Using the emission channeling technique at the ISOLDE/CERN facility, we determined the lattice location of ^{11}Be ($t_{1/2} = 13.8$ s) in different doping types of GaN as a function of implantation temperature. We find within an accuracy of 0.08 Å that the location of interstitial Be is the one predicted by theory. The room temperature interstitial fraction of ^{11}Be was correlated with the GaN doping type, being highest (up to ∼80%) in *p* type and lowest in *n*-GaN, thus giving direct evidence for the amphoteric character of Be. We find that interstitial ^{11}Be fractions are generally much higher than for Mg, which confirms that indeed self-compensation should be considerably more pronounced for Be. With rising implantation temperature, an increasing conversion of interstitial to substitutional Be is observed, involving at least two clearly identifiable steps at 50–150 °C and 350–500 °C. This suggests that the migration of interstitial Be may be subject to two different activation energies.

DOI: 10.1103/PhysRevB.105.184112

I. INTRODUCTION

Gallium nitride is a wide band gap semiconductor that has revolutionized solid state lighting technology and is nowadays also increasingly used for power electronics devices. One of the breakthroughs that paved the way for technological applications of GaN was the realization of *p*-type doping by means of Mg in 1989 [1,2]. However, Mg in GaN is a comparatively deep acceptor (acceptor ionization energy $E_A \approx 245$ meV [3]) and suffers from a number of other issues such as hydrogen passivation [4], compensation by native donors [4,5], the tendency of Mg to form clusters [6], or its amphoteric nature [5,7,8], that all limit the achievable free hole concentrations. Therefore, intensive research for alternative *p*-type dopants that might present shallower energy levels has been on the way, and Be, like Mg, an element from group II of the periodic table, has been one of the candidates investigated. However, experimentally, Be-doped GaN has been found to be highly compensated [9] or semi-insulating [10–16], indicating the compensation of Be acceptors by donor-type defects, although the nature of the latter remained unclear.

From the theoretical side, Be is one of the most studied impurities in GaN and considerable efforts have been made in order to understand its doping behavior [4,16–32]. However, up to now no consensus has been reached regarding theoretical predictions of its acceptor level(s), for which values of <200 meV [16], 60 meV [17], 185–241 meV [18], 183–190 meV [20], 60 meV [22], 120 meV [23], 550 meV [25], 47–93 meV [26], 600 meV [28], 720–800 meV [29], and 205 meV [31] can be found in the literature. One theoretical study [24] and recent experimental results [30] point towards the hypothesis that Be has two acceptor levels, a relatively shallow one ($E_A \approx 113$ meV), and a second, which is deeper ($E_A \approx 580$ meV) and characterized by large lattice relaxations. Moreover, several theoretical studies [4,16,19,21–23,25,31] have predicted that Be is an amphoteric impurity in GaN, meaning that it can occupy substitutional Ga positions (Be_{Ga}), where it acts as an acceptor, but also interstitial sites (Be_i), where it acts as a double donor. This implies that the formation of interstitial Be_i instead of substitutional Be_{Ga} should become more favorable in *p*-GaN, which was forecast to be the case once the Fermi level is closer than ≈1.2 eV [16], 0.8 eV [19], 0.5 eV [21], 0.3–0.5 eV [22], 1.4–1.8 eV [25], or 1.2–1.6 eV [31] from the valence band. The lack of *p*-type characteristics following Be doping could thus be explained by self-compensation, i.e., by the incorporation of similar amounts of Be_{Ga} and Be_i, with the additional possibility of the formation of electrically inactive Be_i-Be_{Ga} complexes. However, for the existence of interstitial Be, despite being predicted by theory, no direct experimental evidence was given so far. The only indication comes from positron annihilation

*Corresponding author: uwahl@ctn.tecnico.ulisboa.pt

spectroscopy experiments [33], where it was found that in Be-doped GaN, following prolonged high-temperature annealing around 900 °C, an increased amount of Ga vacancies V_{Ga} was detected. The authors suggested that substitutional Be_{Ga} was converted to interstitial Be_i according to the reaction $Be_{Ga} \rightarrow Be_i + V_{Ga}$ for which an activation energy of 3.5(5) eV was estimated.

Here we present experimental results on the lattice location of ion implanted Be, which clearly establish its amphoteric nature, i.e., we find the coexistence of Be on substitutional Ga and on interstitial sites, with the Be lattice location preference depending on the doping character of the sample. Ion implantation introduces Ga and N vacancies and interstitials into the sample, which may interact with each other to form more complicated defect complexes, but also with the implanted species. In addition, ion implantation is a process out of thermal equilibrium. While one therefore may not expect exactly the same lattice sites occupied by Be as for doping during growth, our results clearly show that the doping type, and hence the position of the Fermi level, influences the Be location *even* following ion implantation. We are also able to experimentally confirm theoretical predictions for the exact location of interstitial Be in the wide-open channels parallel to the *c* axis. Besides, we present estimates for the activation energies of the interstitial migration of Be, which support the suggestion by theory that there exist two different activation energies for Be_i diffusion, one for migration parallel to and the other for migration perpendicular to the *c* axis.

II. METHODS

For lattice location determination of Be, we made use of the electron emission channeling (EC) technique from radioactive isotopes [34–37]. In this experimental method (cf. schematic illustration S1 in the Supplemental Material [38]), radioactive probe isotopes are ion implanted into single-crystalline samples, typically at low fluences of 10^{11}–$10^{13}\,cm^{-2}$. Depending on their chemical nature and experimental conditions, the probe atoms occupy specific lattice sites in the material, on which they subsequently decay by the emission of β^- particles. The β^- particles interact with the crystal potential which guides them on their way out of the sample. This effect results in a pronounced angular dependence of the β^- emission yields around major crystallographic directions that are characteristic for the lattice site(s) that the probe atoms occupied during their decay. The corresponding angular-dependent emission patterns are recorded by means of a two-dimensional position-sensitive detector (PSD) [35,36] which is placed at a suitable distance from the sample. The major lattice sites can be identified by fitting the experimentally observed emission yields by linear combinations of theoretically expected patterns calculated for specific positions of the emitter atoms in the lattice [35,36,39].

The only isotope of Be which is suitable for electron emission channeling lattice location experiments is the short-lived ^{11}Be ($t_{1/2} = 13.81$ s). ^{11}Be was produced at the online isotope separator facility ISOLDE [40] at CERN, by means of 1.4-GeV proton-induced spallation reactions from a UC_2 target. Following out-diffusion from the UC_2 target at high temperature, the ^{11}Be atoms were ionized using a resonant laser ion source [41], electrostatically accelerated and mass separated. ^{11}Be decays by the emission of β^- particles with an end-point energy of 11506 keV (average β^- energy 4652 keV) into stable ^{11}B. Due to the unusually high energies of the emitted β^- particles, which are about a factor of 5–10 higher than for more common EC probe isotopes, emission channeling lattice location experiments with ^{11}Be and their analysis are particularly challenging. Since the angular width of channeling effects scales approximately inversely proportional to the square root of the particle energy, β^- EC effects from ^{11}Be are very narrow (angular widths less than 0.5°), requiring superior angular resolution. The samples were analyzed using a $3 \times 3\,cm^2$ Si pad PSD consisting of 22×22 pixels of size $1.3 \times 1.3\,mm^2$, which was placed 60 cm from the sample, resulting in an angular range of ±1.36°. While the comparatively large distance from sample to detector guarantees sufficient angular resolution (0.05° standard deviation), it results in a relatively small solid angle of detection, so that during Be beam times fewer measurements can be performed than in the case of other isotopes such as, e.g., ^{27}Mg in GaN [7,8].

Moreover, the analysis of EC patterns from ^{11}Be is also challenging since the computational effort required to calculate theoretical emission patterns by means of the "many-beam" formalism grows considerably as a function of the electron energy. Angular emission patterns from 200–250 different lattice sites in the wurtzite structure were calculated around the major crystallographic directions in the *x* and *y* directions from −3° to +3° in steps of 0.025°. More details on the corresponding many-beam calculations are given in the Supplemental Material [38].

Three of the samples were epilayers grown at the University of Cambridge: a not intentionally doped GaN (nid-GaN no. 1), an *n*-GaN:Si layer doped with $1 \times 10^{19}\,cm^{-3}$ Si, and a *p*-GaN:Mg layer doped during growth with $2 \times 10^{19}\,cm^{-3}$ Mg and annealed for 20 min at 800 °C under nitrogen atmosphere in order to drive out H and electrically activate the Mg (typical hole concentrations $1–2 \times 10^{17}\,cm^{-3}$ and Hall mobilities $10–15\,cm^2/V\,s$ [42]). In addition, two undoped layers (nid-GaN no. 2 and no. 3) from other suppliers were used during exploratory measurements. The characteristics of the different samples are described in more detail in the Supplemental Material [38].

The EC measurements were performed during 30-keV implantations of $^{11}Be^+$ using the online setup described in Ref. [43]. The ^{11}Be implantation profiles are approximately Gaussian with mean depth and straggling around 900 (400) Å [44], varying somewhat due to the fact that different implantation angles towards the surface normal are required for online detection of the channeling effects from the various crystallographic directions. The typical beam current into the 1-mm-diameter beam spot was around 1.1 pA, corresponding to 7×10^6 atoms/s and a fluence rate of $9 \times 10^8\,atoms/cm^2/s$.

For the analysis of the experimental patterns, these were fitted [35,39] by a linear combination of substitutional and interstitial ^{11}Be emitter atoms. In order to identify the most likely interstitial Be_i site, its position was varied and the chi square of fit used as a criterium.

When measuring electron emission channeling effects the recorded angular anisotropy is always subject to background, which arises mostly from two sources: (a) electrons which undergo large-angle scattering inside the sample, the substrate, the sample holder, or on the walls of the vacuum chamber and hence do not contribute to the channeling effect, and (b) gamma radiation. The latter may be emitted by the sample itself and thus reach the detector directly, or from ^{11}Be atoms which are deposited on the collimator nozzle and whose gamma radiation reaches the detector through the shielding in between nozzle and detector, or result from other radioisotopes in the vicinity of the detector. Both electron and gamma background were taken into account in the analysis, by multiplying fitted fractions with a background correction factor of 1.8 (details on the derivation of the background correction factor can be found in the Supplemental Material [38]). This allowed estimating "absolute" fractions on substitutional and interstitial sites, f_S and f_i, as are given below in Figs. 1 and 2. Typically, the error in the sum fractions $f_{sum} = f_S + f_i$ of identified sites is in the 10–15% range, and an overestimation of background may then cause the sum of identified fractions to be somewhat larger than 100%. In online experiments with short-lived isotopes, a complication arises from the fact that changes in beam characteristics may lead to a variation of the distribution of radioactive probe atoms deposited on the sample and on the nozzle. For the case of ^{11}Be, where the vacuum valves to the production target have to stay constantly open, an additional problem is background from radioactive noble gases. Proton impact on the UC_2 targets also produces isotopes of radioactive noble gases, which can out-diffuse and migrate through the beam lines [45], thus reaching the vicinity of the detector. Changes in beam characteristics and radioactive noble gas background cause variations in the gamma background of the order of 5–10% which would be reflected as proportional variations in both the derived fractions f_S and f_i on substitutional and interstitial sites. Such variations can be eliminated by considering not the absolute but the relative fractions of substitutional or interstitial sites, e.g., $f_i/(f_S + f_i)$. This approach has been chosen for the data presented in Figs. 6 and 7, when assessing the amount of interstitial Be as a function of implanted fluence and implantation temperature, respectively.

III. RESULTS AND DISCUSSION

In Figs. 1(a)–1(d) we have displayed the normalized angular distributions of β^- particles emitted around the [0001], [$\bar{1}$102], [$\bar{1}$101], and [$\bar{2}$113] directions of the *p*-GaN:Mg sample during room temperature (RT) implantation of ^{11}Be. The best fits of theoretical patterns [Figs. 1(e)–1(h)] are represented by a linear combination of theoretical patterns from ^{11}Be on substitutional Ga and interstitial Be_i sites, which, following background correction, correspond to fractions of $f_S = 38\%$ and $f_i = 65\%$, hence with the majority on interstitial sites. Figures 2(a)–2(d) show experimental patterns around the same four axial directions as Fig. 1, but for the implantation temperature $T_i = 800\,^{\circ}$C. In this case, the fit procedure resulted in background-corrected fractions of 97% on substitutional Ga sites and 4% on interstitial positions [Figs. 2(e)–2(h)]. Patterns for RT and 600 °C implantations in samples nid-GaN no. 1 and no. 3 are shown in Figs. S9–S11 of the Supplemental Material [38]. The procedure of how the exact location of the best fit Be_i position was determined will be discussed below.

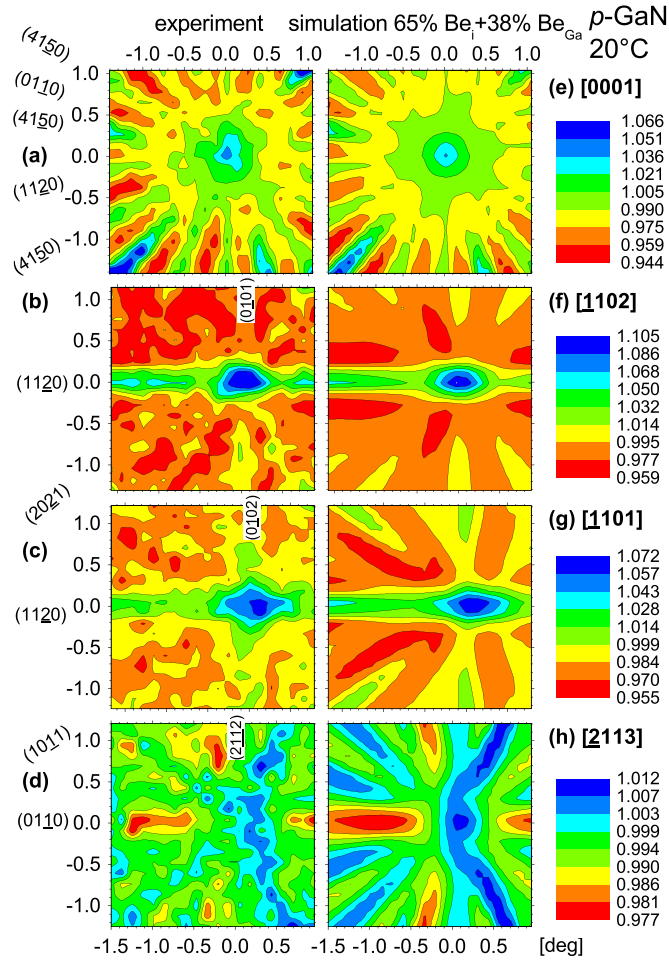

FIG. 1. (a)–(d) Angular distribution of β^- emission yields from ^{11}Be in *p*-GaN:Mg, measured during RT implantation. (e)–(h) The best fits of simulated patterns, corresponding to 65% on Be_i interstitial and 38% on substitutional Ga sites. The major planar directions are indicated. Number of detector events per experimental pattern: (a) 1.7×10^7, (b) 4.3×10^6, (c) 4.3×10^6, (d) 9.7×10^6.

The considerable amount of ^{11}Be on interstitial sites at RT is qualitatively illustrated by the following. The [0001] pattern in Fig. 2(a) for 800 °C implantation is dominated by substitutional sites, for which the sets of planar directions (11$\bar{2}$0) and (01$\bar{1}$0) exhibit a rather similar intensity of channeling effects, with (11$\bar{2}$0) being somewhat more intense than (01$\bar{1}$0) [Fig. 3(e) and Fig. S5(e) of the Supplemental Material [38]]. Channeling effects from the minor planes (41$\bar{5}$0) are invisible in this case. For interstitial sites, the [0001] and [$\bar{2}$113] axial and the planar (01$\bar{1}$0) effects are characterized by emission minima rather than channeling effects [Figs. 3(a), 3(d), S5(a), and S5(d)]. Therefore, the channeling intensities of these directions are considerably reduced for RT implantation when mostly interstitial sites are occupied: in Fig. 1, which is dominated by Be_i interstitial sites, in panel (a) the anisotropy of the axial [0001] effect is around 25% of that in

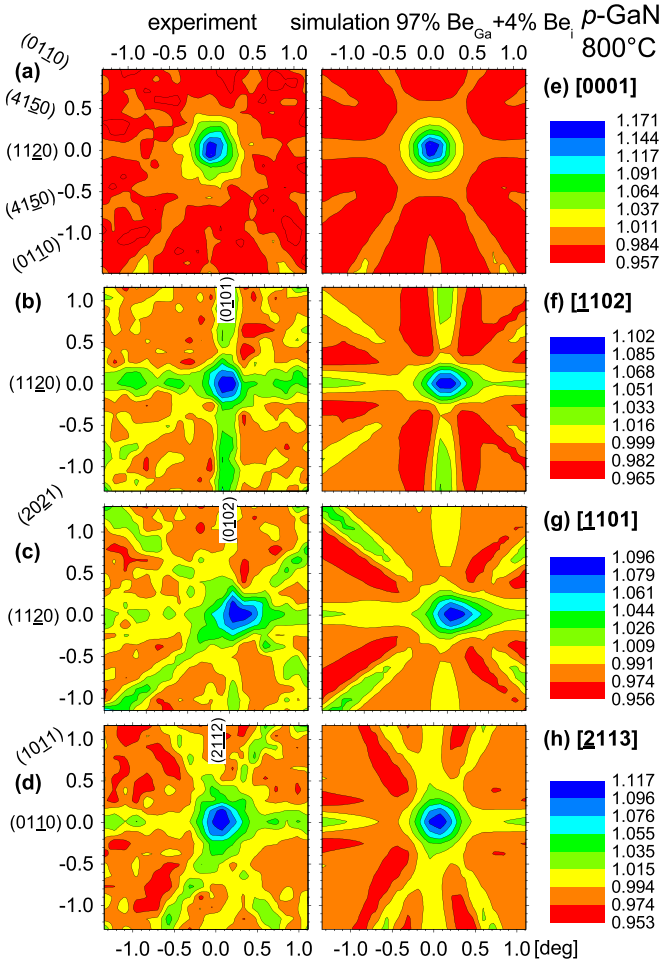

FIG. 2. (a)–(d) Angular distribution of β^- emission yields from ^{11}Be in *p*-GaN:Mg, measured during implantation at 800 °C. Panels (e)–(h) show the best fit of simulated patterns, corresponding to 97% on substitutional Ga and 4% on Be$_i$ interstitial sites. Note that the azimuthal orientation of the [0001] pattern differs by 12° from the one shown in Fig. 1(a). Number of detector events per experimental pattern: (a) 3.0×10^6, (b) 2.7×10^6, (c) 3.3×10^6, (d) 3.4×10^6.

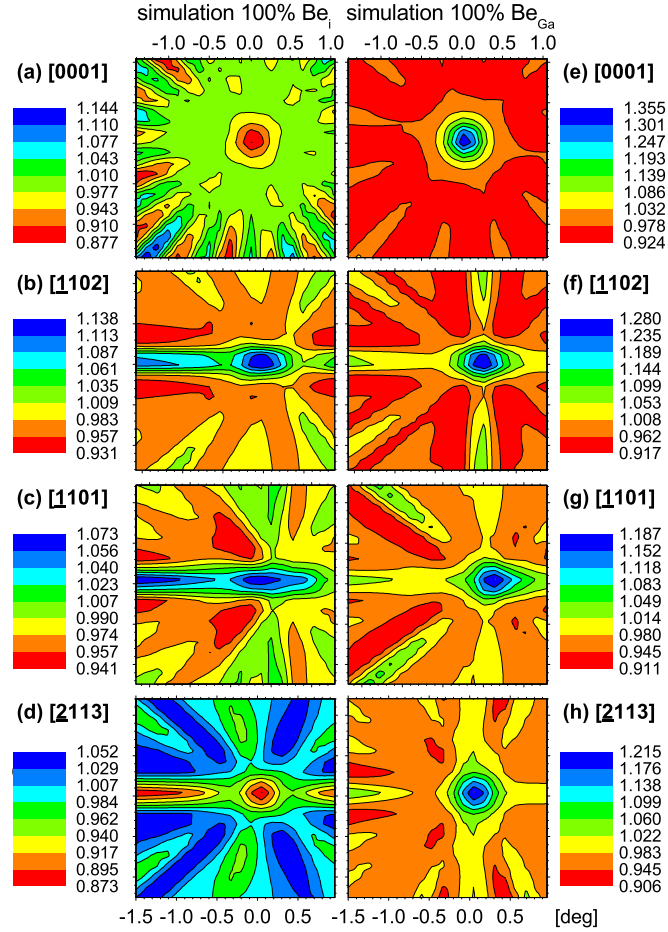

FIG. 3. Simulated β^- emission channeling patterns for 30-keV implanted ^{11}Be in GaN along the four major crystallographic directions. Panels (a)–(d) are patterns for 100% of emitter atoms on the Be$_i$ interstitial sites, i.e., shifted by +0.69 Å from ideal O sites via HB towards the HAB position, while (e)–(h) are for 100% on substitutional Ga sites. Note that the orientation of all patterns has been chosen so as to correspond to the measurements at RT as shown in Figs. 1(a)–1(d). The occupation of substitutional Ga sites results in distinct channeling effects along all major axial and planar directions. The clearest distinction between Be$_{Ga}$ and Be$_i$ sites is visible in the [0001] and [$\bar{2}$113] patterns. For Be$_i$ sites the axial [$\bar{2}$113] effect, and the set of (01$\bar{1}$0) planes, located under angles of −42°, +18°, and +78° from the horizontal in (a), and horizontally in (d), are characterized by blocking minima. Note that a version of this figure with all major planes indicated can be found in Fig. S5 of the Supplemental Material [38].

Fig. 2(a). In addition, the (01$\bar{1}$0) planes [Figs. 1(a) and 1(d)] and the [$\bar{2}$113] axis [Fig. 1(d)] show minima. On the other hand, since along [$\bar{1}$102] and [$\bar{1}$101] half of the projections of the Be$_i$ interstitial sites are approximately aligned with atomic rows of Ga (cf. Fig. S3 of the Supplemental Material [38]), the corresponding calculated patterns show channeling effects along these directions [Figs. 3(b) and 3(c)], with maxima that correspond to roughly half the anisotropy resulting from the occupation of substitutional Ga sites.

Note that [0001] patterns do not allow us to pinpoint the position of the Be$_i$ interstitials *parallel* to the *c* axis; this can only be accomplished from analyzing patterns measured off the *c* axis, i.e., in our case [$\bar{1}$102], [$\bar{1}$101], and [$\bar{2}$113]. For this purpose, we have adopted the following procedure. For each pattern two-site fits were performed, where the first site was kept fixed at the substitutional Ga position, while the position of the second, interstitial site was varied in small steps parallel to the *c* axis in the center of the wide-open space. As step width we used 0.0162 Å in between HA and HB sites (i.e., in the vicinity of the ideal O position), and 0.0486 Å in between HA or HB and HAB. The resulting χ^2 of fit were normalized to those of one-site fits with substitutional Ga sites only. The results are shown in Fig. 4. In the case of the nid- and *p*-GaN samples implanted at room temperature, which both showed relatively large fractions of Be$_i$, distinct minima in the relative χ^2 were grouped in a relatively narrow region around a position +0.69(8) Å from ideal O sites, i.e., in between the HB and HAB sites. In the case of the *n*-GaN sample, unfortunately only the [$\bar{1}$102] and [$\bar{1}$101] direction could be measured, and the results are less clear. First, the variations in

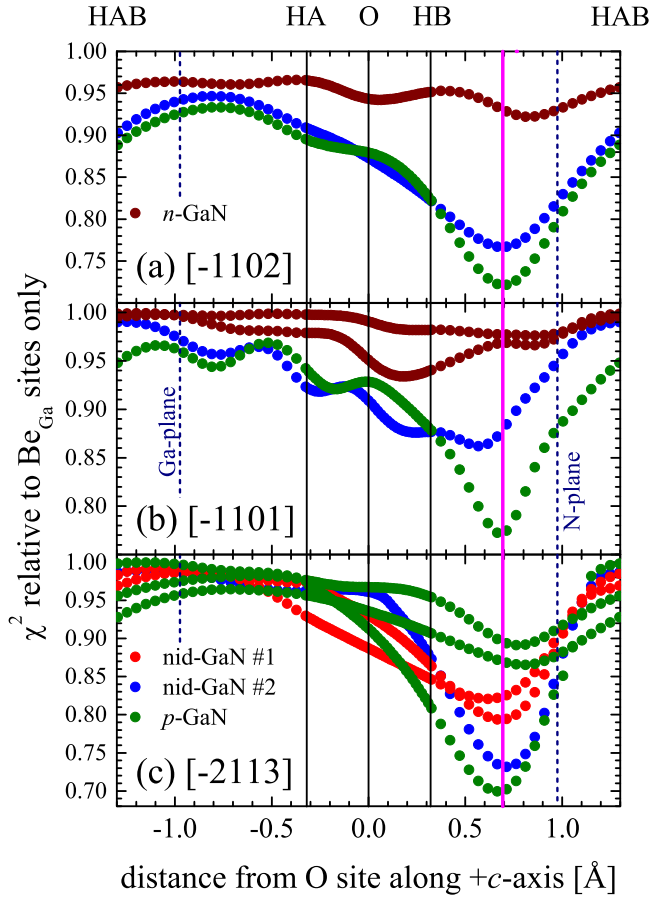

FIG. 4. Relative χ^2 of the fits to the experimental [$\bar{1}$102], [$\bar{1}$101], [$\bar{2}$113] patterns from room temperature implantation of ^{11}Be in GaN as a function of displacement of the ^{11}Be atoms from the ideal interstitial O sites parallel to the c axis. Each data point corresponds to the χ^2 of the best fit obtained using two given sites, with the corresponding two fractions as free parameters. The site pairs are composed of a fixed substitutional Ga site plus a second site, which is shifted from the ideal interstitial O site along the c axis. The relative χ^2 values were normalized to that of the one-site substitutional Ga fit. The black vertical lines indicate the positions of the HA, O, and HB interstitial sites. The magenta-colored vertical line shows the average of the best fit positions from the nid- and p-GaN samples.

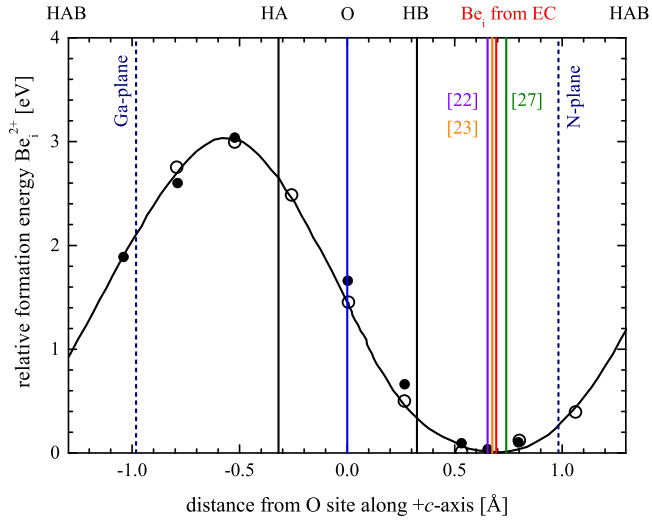

FIG. 5. The open and closed circles show the calculated relative formation energy of Be_i^{2+} interstitials at various positions within the open channel parallel to the c axis of the GaN wurtzite lattice using two different k meshes, with the solid line interpolated values, as given in Fig. 8 of Ref. [22]. The dashed blue vertical lines represent the positions of the Ga and N planes perpendicular to the c axis, while the violet, orange, and green vertical lines indicate the positions of Be_i minimum total energy predicted in Refs. [22,23,27], respectively. The Be_i position that resulted in the overall best fits of EC data from this work is shown as the vertical red line.

the relative χ^2 are less pronounced since in n-GaN, as will be shown below, fewer ^{11}Be probe atoms occupy the interstitial sites, leading to a smaller improvement in fit quality when interstitial positions are allowed in the fit. Second, two of the three measurements performed show minima close to the Be_i position identified for the nid- and p-GaN samples, with less pronounced minima in between the O and HB sites. The third measurement shows the minimum about midway between O and HB sites, with a weaker minimum near the Be_i position. While this may be an artefact of this particular measurement, the possibility cannot be ruled out that there are two types of interstitial sites occupied in the n-GaN sample. However, the approach of using three-site fits gave ambiguous results, and this could not be confirmed.

Figure 5 displays the predicted relative energy of formation of Be_i in GaN (with respect to the minimum value found) as a function of the position parallel to the c axis (with the origin of the length scale on ideal O sites), as reported by Van de Walle *et al.* [22] from their first principle density functional calculations. Shown as colored vertical lines are the theoretically predicted minimum energy positions of Be_i, which are +0.65 Å [22], +0.68 Å [23], and +0.74 Å [27] from O sites, as well as at +0.69(8) Å, the most likely position identified from the emission channeling lattice location, as described above. As can be seen, the theoretical predictions agree quite well with each other and the Be_i position obtained from emission channeling experiments.

In Fig. 6 we show the derived relative fractions of interstitial Be_i, $f_i/(f_S + f_i)$, for RT implantations as a function of recorded events in the detector. Each data point corresponds to ~280 000 detector events, which is equivalent to an implanted ^{11}Be fluence of 1.8×10^{11} cm^{-2}. As is clearly visible the highest amount of interstitial Be is obtained in p-GaN, where at the beginning of the implantations into each fresh beam spot values around 65–80% are reached. As the implanted fluence increases, the amount of interstitial Be_i decreases, while it is also subject to fluctuations that can reach more than ±10%. As was previously discussed for the case of ^{27}Mg [8], the rapid fluctuations are probably related to the quasiperiodic buildup of positive surface charges resulting from the positive charge of the implanted Be^+ ions, secondary electron emission during the implantation process, as well as β^- particles emitted from the sample. This may lead to quasiperiodic fluctuations of the Fermi level in the near-surface region. These fluctuations are averaged out by measuring for longer time intervals or by smoothing the raw data points, as shown by the red curves in Fig. 6. The amount of interstitial Be is

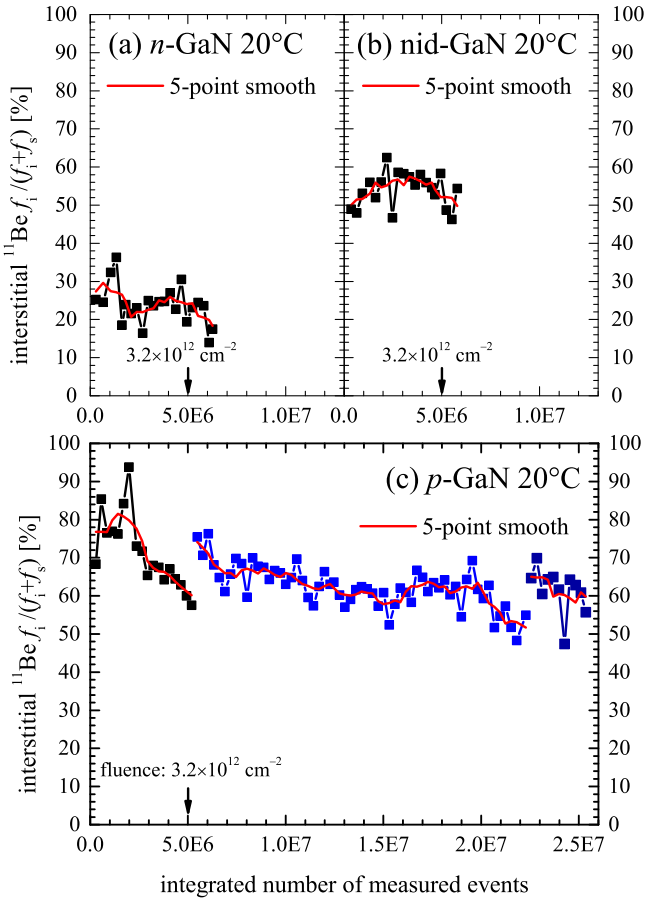

FIG. 6. Relative amounts of interstitial $^{11}Be_i$ for RT implantation as a function of the integrated number of measured events in (a) *n*-GaN, (b) nid-GaN, and (c) *p*-GaN. The red lines in the plots were obtained by performing five-point smooths on the raw data points. Every 5×10^6 events correspond to an implanted ^{11}Be fluence of 3.2×10^{12} cm^{-2}, as indicated by the black arrows. Note that in panel (c) for each of the three data sets a fresh beam spot was chosen, thus the overall number of implanted Be atoms did not accumulate in a single spot on this sample.

lowest in *n*-GaN, reaching only values around 30% at the beginning of the implantation, and dropping to ∼20% for 3.8×10^{12} cm^{-2}. The prevalence of interstitial vs substitutional Be in *p*-type GaN clearly illustrates the amphoteric character of Be, as it was predicted by theory that interstitial Be should be more abundant when the Fermi level is close to the valence band. As was already explained for the case of ^{27}Mg [8], prolonged implantations, in this case of Be, lower the interstitial fractions of amphoteric dopants in *p*-type GaN since the radiation damage introduced by implantation has a compensating effect, i.e., the Fermi level moves upward and the material loses its *p*-type character. Moreover, in all doping types, with increasing Be fluence the accumulation of Ga vacancies V_{Ga} makes it more likely that freshly implanted ^{11}Be atoms during their slowdown find a V_{Ga} to combine with and thus become Be_{Ga}. Since the amount of V_{Ga} introduced into the samples by Be implantation influences the fractions of substitutional Be, one may wonder whether the initial, native concentrations of V_{Ga} differ between *n*-and *p*-type material, and how this could possibly influence the outcome of the experiment. As a matter of fact, by means of positron annihilation spectroscopy (PAS), native V_{Ga} concentrations were found to depend on the type of doping and the growth method [46–49]. V_{Ga} could never be detected ($<10^{16}$ cm^{-3}) in *p*-GaN [47,48], while in not intentionally doped *n*-type GaN grown by metalorganic-chemical-vapor deposition (MOCVD) [V_{Ga}] was reported often as high as 10^{17}–10^{18} cm^{-3} [46,48], but could be varied in between 10^{16} cm^{-3} and 10^{19} cm^{-3} by means of choosing the N/Ga molar ratio during growth [47]. On the other hand, in *n*-GaN intentionally doped with Si during MOCVD growth, only up to 5×10^{16} cm^{-3} V_{Ga} were found [48]. In our case, the native V_{Ga} concentrations are probably of minor importance for the outcome of the experiment. As estimated by SRIM simulations [44], 30-keV implantation of 3.2×10^{12} cm^{-2} ^{11}Be creates a peak concentration of 4.8×10^{19} cm^{-3} V_{Ga} (before thermalization), which is quite above the values reported for typical native samples. In Mg-implanted GaN, PAS identified the double vacancy ($V_{Ga}V_N$) as a major positron-trapping defect species, although concentrations could not be quantified [49].

Figure 7 shows the derived relative fractions of interstitial Be_i, $f_i/(f_S + f_i)$, as a function of implantation temperature for three samples of different doping types. These were obtained by measuring only the [0001] pattern from each sample and increasing the implantation temperature without changing the sample orientation, i.e., the beam spots on the samples were left unchanged. Also, due to the longer measuring times at each temperature, initial transients and fluctuations, such as are observed in Fig. 6, are averaged out. First, we note that for RT implantation, relative interstitial fractions are highest in *p*-GaN (∼57%), somewhat lower (∼50%) in nid-GaN, while being considerably smaller (∼25%) in *n*-GaN. As a general trend, with increasing implantation temperature, the amount of interstitial Be was reduced in all samples, however, not in a monotonous way. In each case there are two steps visible. A first, smaller step is observable in all samples in between 50 and 150 °C. Above this step, the interstitial fractions even seem to increase somewhat again until at around 350 °C the second, most prominent step is reached. This slight rise, which is not very obvious here, was observed much more pronounced in the case of ^{27}Mg, where it was attributed to the fact that with increasing implantation temperature the amount of produced Ga vacancies is reduced, thus providing less possibilities for substitutional incorporation of the implanted Mg [7,8]. Following the 350–500 °C step, the relative interstitial fractions are not zero, though. In *p*-GaN, where data are available up to 800 °C, Be_i was further reduced rather monotonously to a few percent only. A similarly low fraction was reached in nid-GaN already by implanting at 600 °C. For *n*-GaN, the highest implantation temperature investigated was 500 °C, which reduced the relative interstitial fraction to ∼10%. Assuming that the steps are due to the reaction $Be_i + V_{Ga} \rightarrow Be_{Ga}$, where mobile Be_i interstitials migrate until after a number of jumps N they encounter a Ga vacancy V_{Ga}, the various steps were fitted using the following Arrhenius approach, as was described in more detail in Refs. [7,8]

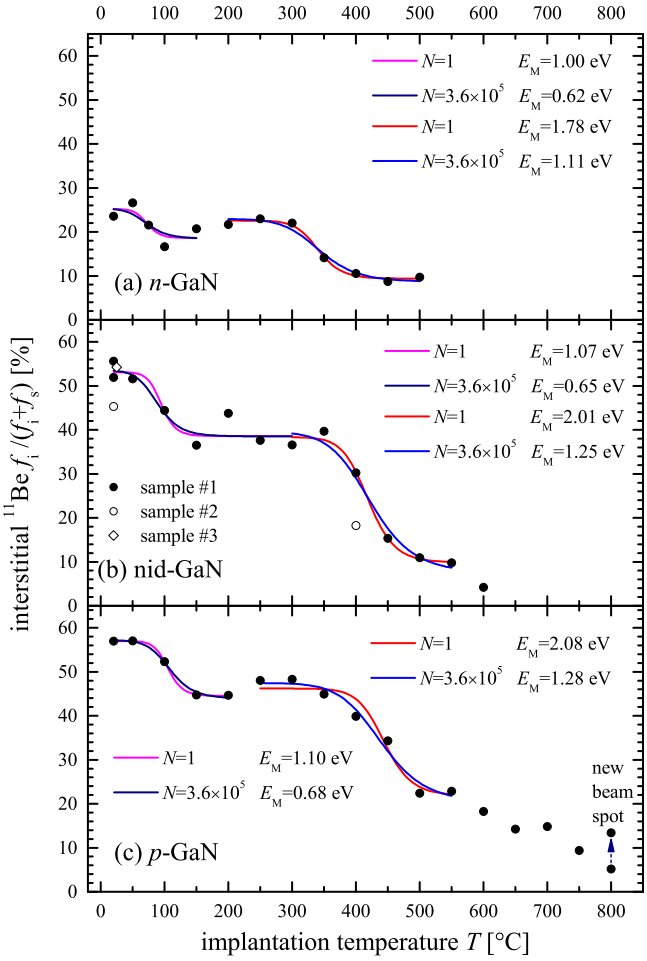

FIG. 7. Relative amounts of interstitial ^{11}Be as a function of implantation temperature in the three doping types of GaN investigated. Each data point corresponds to (a) $\sim 1.0 \times 10^6$, (b) $\sim 1.2 \times 10^6$, (c) $\sim 2.1 \times 10^6$ detector events. The colored lines represent fits of two Arrhenius models for the site changes of interstitial ^{11}Be to substitutional positions, as is described in more detail in the text, performed for the temperature range around 400 °C where the most prominent step occurs, and for the minor step around 100 °C. The number of jumps N of Be_i considered in the models is either $N = 1$ or $N = 3.6 \times 10^5$, while E_M are the corresponding best fit values for the interstitial migration energy.

for the case of ^{27}Mg:

$$f_i(T) = (f_{i0} - f_{i\infty}) \frac{1}{1 + \frac{\nu_0 \tau}{N} e^{-E_M/k_B T}} + f_{i\infty}. \qquad (1)$$

f_{i0} and $f_{i\infty}$ are the interstitial fractions at temperatures below and above the step, ν_0 is the jump attempt frequency, $\tau = 19.9$ s is the radioactive lifetime of ^{11}Be, and E_M is the activation energy for migration of interstitial $^{11}Be_i$. Taking the attempt frequency $\nu_0 = 2 \times 10^{13}$ Hz [7], N was assumed either to be 1 (V_{Ga} immediately neighboring $^{11}Be_i$) or 3.6×10^5 (the upper limit when the diffusion-induced broadening of the ^{11}Be profile would become comparable to the implantation depth) and least square fits were performed on the data sets in Fig. 7.

The best fit curves to $f_i/(f_S + f_i)$, assuming the functional relationship of Eq. (1), have been included in Fig. 7, as well as the corresponding migration energies E_M. As can be seen, there are only small differences in the best fit values for E_M, being 1.00–1.10 eV ($N = 1$) and 0.62–0.68 eV ($N = 3.6 \times 10^5$) for the step around 50–150 °C, and 1.78–2.08 eV ($N = 1$) and 1.11–1.28 eV ($N = 3.6 \times 10^5$) for the step around 350–500 °C. Our estimates for E_M related to the two steps fall close to the range of values predicted by theory for migration of interstitial Be_i^{2+} in GaN perpendicular and parallel to the c axis, respectively, which are $E_{M\perp} = 1.18$ eV and $E_{M||} = 2.90$ eV [21,22], and $E_{M\perp} = 0.76$ eV and $E_{M||} = 1.88$ eV [27]. A probable explanation for the two steps is hence that the first step around 50–150 °C is related to migration of $^{11}Be_i$ perpendicular to the c axis, while the second step around 350–500 °C represents $^{11}Be_i$ migration parallel to it.

Assuming this interpretation is correct, it may seem surprising that the step at 50–150 °C does not lead to a more severe drop in the interstitial Be fraction, since it should result in long-range diffusion. However, if in this case the migration of each ^{11}Be probe is confined to one specific interstitial plane perpendicular to the c axis, i.e., parallel to the surface, the chance of encountering Ga vacancies within that plane is limited, and it may be that a considerable number of implanted ^{11}Be ions do not encounter a V_{Ga} during their lifetime.

It is worthwhile mentioning that the energies for interstitial migration E_M estimated from emission channeling experiments of ^{8}Li, ^{24}Na and ^{27}Mg in GaN and ^{24}Na and ^{27}Mg in AlN were found to be correlated with the ionic radii of Li^+, Na^+, and Mg^{2+} [50] and in agreement with most theoretical predictions. The data presented here for the case of Be^{2+} further confirm this trend: due to having the smallest ionic radius of 0.41 Å, Be^{2+} is the fastest interstitial diffuser among these alkaline-metal and alkaline-earth-metal ions.

In the p-GaN sample there is still a continuous decrease in f_i between 550 and 800 °C. Such a behavior would be understandable if there were a process that slows down the migration for part of the interstitial Be, such as being bound to other defects, so that for some Be interstitials a higher activation energy is required to combine with Ga vacancies. On the other hand, since the beam spot was left unchanged, there is also the effect that with each new measurement temperature the sample has reached a higher implanted fluence of Be, which may lower the interstitial fractions due to the introduction of Ga vacancies. In order to test for this effect, following the last measurement of the p-GaN sample at 800 °C, a new beam spot was chosen and the pattern remeasured at the same temperature. This increased the relative interstitial fraction of Be from 5% to 13%, which shows that there exists a fluence effect even at this high temperature. Considering that the first measurement at 800 °C took place on the beam spot that had accumulated Be implantations from all previous measurements at lower temperatures, amounting to a fluence of 2.3×10^{13} cm^{-2}, obviously not all of the accumulated damage had been removed at this temperature.

As was briefly mentioned in the Introduction, it was suggested from positron annihilation spectroscopy experiments [33] that prolonged (2 h) annealing at 900 °C causes substitutional Be_{Ga} to leave its lattice site and become interstitial

according to the reaction $Be_{Ga} \rightarrow Be_i + V_{Ga}$. In principle this should be detectable with the emission channeling method as well, however, our experimental setup does not allow extended measurements at such a high temperature, and due to the short half-life of ^{11}Be (13.81 s), even higher temperatures would be required to achieve the same effect as a 2-h anneal at 900 °C. Hence we could not explore this reaction.

Several theoretical papers [22,24,28–30] have predicted that neutral substitutional Be_{Ga}^0 is subject to large lattice relaxations, which cause it to be substantially displaced from the ideal Ga site along the *c* axis towards the antibonding ABA position. Note that Be_{Ga}^0 should be only found in *p*-type GaN, once the Fermi level is close to the valence band. While the predicted elongation of the Be^0-N bond along the *c* axis is in the range 0.3–0.8 Å [22,28–30], only in one case is the displacement of Be from the ideal Ga position explicitly stated (0.21 Å [22]). We have hence examined our data for signs of such displacements, but there was no firm evidence that the implanted ^{11}Be probes that are found on substitutional sites, or a significant fraction of them, are displaced. However, since the Fermi level may not have been sufficiently close to the valence band to form Be_{Ga}^0 under our experimental conditions, this does not rule out the existence of the displacements.

Comparing Be to the major *p*-type dopant Mg, we note the following qualitative similarities and quantitative differences. While both light group II atoms can occupy substitutional Ga and interstitial sites, the amphoteric character of Be is considerably more pronounced. Interstitial fractions of ^{11}Be were found substantially higher than previously for the case of ^{27}Mg [7,8], which supports theoretical predictions [4,16,19,21–23,25,31] that Be is more prone to self-compensation and thus unsuitable for *p*-type doping. The exact locations of the interstitial sites of Mg parallel to the *c* axis [−0.60(14) Å from the O site in *p*-GaN] and Be [+0.69(8) Å] differ, with Be_i located closer to the N atoms. This experimental result is partially understandable by the fact that Be^{2+} is a smaller ion than Mg^{2+} (0.41 Å vs 0.71 Å), and hence can move closer to the electronegative N atoms. However, in the case of Mg there is a discrepancy to theoretical predictions, which expect Mg^{2+} at +0.03 Å [27], i.e., practically at the ideal O site. It is worth mentioning that a recent EC experiment on lattice location of ^{27}Mg in *n*-GaN grown on Si pointed at a location of −0.14(5) Å [51], hence it seems possible that the interstitial positions change somewhat in different kinds of samples. This would need further investigation.

Both Mg and Be show fast interstitial diffusion, making them, in interstitial form, quite mobile in GaN at 500 °C. However, while for Be we could identify two steps in the onset of interstitial mobility (around 50–150 °C and 350–500 °C), in the case of Mg there was only one around 350–500 °C [7,8]. This behavior is understandable, if in the case of Be the first step corresponds to interstitial migration perpendicular and the second parallel to the *c* axis, as was discussed in more detail above. In the case of Mg, theoretically predicted migration energies are $E_{M\perp} = 2.20$ eV and $E_{M||} = 2.01$ eV [27], hence quite similar for migration perpendicular and parallel to the *c* axis, meaning that only a single step for the onset of interstitial diffusion should be visible in emission channeling experiments.

IV. CONCLUSIONS

We have provided direct evidence that Be is an amphoteric dopant in GaN. It can occupy substitutional Ga as well as interstitial sites, and its lattice site preference depends on the GaN doping type. Whereas in *p*-GaN and in nid-GaN the majority of implanted ^{11}Be was found on interstitial sites, its amount was significantly less in *n*-GaN. The interstitial fractions of ^{11}Be were considerably higher than those previously found for the case of ^{27}Mg [7,8], which indicates that the amphoteric character of Be is indeed more pronounced than for Mg, thus giving a possible explanation for why it seems impossible to dope GaN *p*-type with Be [4,16,19,21–23,25,31].

We identified the position of Be_i in the wide-open interstitial region at a distance of +0.69(8) Å from ideal O sites, which is in excellent agreement with theoretical predictions [22,23,27].

With increasing implantation temperature, interstitial Be changes its lattice site towards substitutional Ga sites. Two distinct steps, around 50–150 °C and 350–500 °C, were found for this process, and the corresponding interstitial migration energies were estimated from assuming thermally activated Arrhenius behavior. The estimated migration energies of 0.62–1.10 eV and 1.11–2.08 eV are within the range of theoretical predictions made for migration of Be perpendicular and parallel to the *c* axis, respectively [21,22,27].

ACKNOWLEDGMENTS

The authors acknowledge the support of the ISOLDE Collaboration and technical teams. This work was funded by the Portuguese Foundation for Science and Technology (Fundação para a Ciência e a Tecnologia, FCT, CERN/FIS-TEC/0003/2019), the Research Foundation-Flanders (FWO), and the KU Leuven (BOF program). The EU Horizon 2020 Framework supported ISOLDE beam times through Grant Agreement No. 654002 (ENSAR2). T.A.L.L. acknowledges the support by FWO (Projects No. 29681 and No. 52152).

[1] H. Amano, M. Kito, K. Hiramatsu, and I. Akasaki, P-type conduction in Mg-doped GaN treated with low-energy electron beam irradiation (LEEBI), Jpn. J. Appl. Phys. **28**, L2112 (1989).

[2] H. Amano, Nobel lecture: Growth of GaN on sapphire via low-temperature deposited buffer layer and realization of *p*-type GaN by Mg doping followed by low-energy electron beam irradiation, Rev. Mod. Phys. **87**, 1133 (2015).

[3] S. Brochen, J. Brault, S. Chenot, A. Dussaigne, M. Leroux, and B. Damilano, Dependence of the Mg-related acceptor ionization energy with the acceptor concentration in p-type GaN

layers grown by molecular beam epitaxy, Appl. Phys. Lett. **103**, 032102 (2013).

[4] C. G. Van de Walle and J. Neugebauer, First-principles calculations for defects and impurities: Applications to III-nitrides, J. Appl. Phys. **95**, 3851 (2004).

[5] G. Miceli and A. Pasquarello, Self-compensation due to point defects in Mg-doped GaN, Phys. Rev. B **93**, 165207 (2016).

[6] L. Amichi, I. Mouton, E. Di Russo, V. Boureau, F. Barbier, A. Dussaigne, A. Grenier, P. H. Jouneau, C. Bougerol, and D. Cooper, Three-dimensional measurement of Mg dopant distribution and electrical activity in GaN by correlative atom probe tomography and off-axis electron holography, J. Appl. Phys. **127**, 065702 (2020).

[7] U. Wahl, L. M. Amorim, V. Augustyns, A. Costa, E. David-Bosne, T. A. L. Lima, G. Lippertz, J. G. Correia, M. R. da Silva, M. J. Kappers, K. Temst, A. Vantomme, and L. M. C. Pereira, Lattice Location of Mg in GaN: A Fresh Look at Doping Limitations, Phys. Rev. Lett. **118**, 095501 (2017).

[8] U. Wahl, J. G. Correia, A. R. G. Costa, E. David-Bosne, T. A. L. Lima, G. Lippertz, A. Vantomme, M. R. da Silva, M. J. Kappers, and L. M. C. Pereira, Lattice location studies of the amphoteric nature of implanted Mg in GaN, Adv. Electron. Mater. **7**, 2100345 (2021).

[9] K. Lee, B. VanMil, M. Luo, T. H. Myers, A. Armstrong, S. A. Ringel, M. Rummukainen, and K. Saarinen, Compensation in Be-doped gallium nitride grown by molecular beam epitaxy, Mater. Res. Soc. Symp. Proc. **892**, 729 (2006).

[10] S. Krukowski, M. Bockowski, B. Lucznik, I. Grzegory, S. Porowski, T. Suski, and Z. Romanowski, High-nitrogen-pressure growth of GaN single crystals: Doping and physical properties, J. Phys.: Condens. Matter **13**, 8881 (2001).

[11] T. Suski, E. Litwin-Staszewska, P. Perlin, P. Wisniewski, H. Teisseyre, I. Grzegory, M. Bockowski, S. Porowski, K. Saarinen, and J. Nissilä, Optical and electrical properties of Be doped GaN bulk crystals, J. Cryst. Growth **230**, 368 (2001).

[12] W. R. Willoughby, M. E. Zvanut, J. Dashdorj, and M. Bockowski, A model for Be-related photo-absorption in compensated GaN:Be substrates, J. Appl. Phys. **120**, 115701 (2016).

[13] W. R. Willoughby, M. E. Zvanut, and M. Bockowski, Photo-EPR study of compensated defects in Be-doped GaN substrates, J. Appl. Phys. **125**, 075701 (2019).

[14] H. Ahmad, T. J. Anderson, J. C. Gallagher, E. A. Clinton, Z. Engel, C. M. Matthews, and W. A. Doolittle, Beryllium doped semi-insulating GaN without surface accumulation for homoepitaxial high power devices, J. Appl. Phys. **127**, 215703 (2020).

[15] H. Ahmad, J. Lindemuth, Z. Engel, C. M. Matthews, T. M. McCrone, and W. A. Doolittle, Substantial p-type conductivity of AlN achieved via beryllium doping, Adv. Mater. **33**, 2104497 (2021).

[16] M. Vorobiov, O. Andrieiev, D. O. Demchenko, and M. A. Reshchikov, Point defects in beryllium-doped GaN, Phys. Rev. B **104**, 245203 (2021).

[17] F. Bernardini, V. Fiorentini, and A. Bosin, Theoretical evidence for efficient p-type doping of GaN using beryllium, Appl. Phys. Lett. **70**, 2990 (1997).

[18] F. Mireles and S. E. Ulloa, Acceptor binding energies in GaN and AlN, Phys. Rev. B **58**, 3879 (1998).

[19] J. Neugebauer and C. G. Van de Walle, Chemical trends for acceptor impurities in GaN, J. Appl. Phys. **85**, 3003 (1999).

[20] H. Wang and A. B. Chen, Calculations of acceptor ionization energies in GaN, Phys. Rev. B **63**, 125212 (2001).

[21] S. Limpijumnong, C. G. Van de Walle, and J. Neugebauer, Stability, diffusion, and complex formation of beryllium in wurtzite GaN, Mat. Res. Soc. Symp. Proc. **639**, G4.3.1 (2001).

[22] C. G. Van de Walle, S. Limpijumnong, and J. Neugebauer, First-principles studies of beryllium doping of GaN, Phys. Rev. B **63**, 245205 (2001).

[23] C. D. Latham, R. M. Nieminen, C. J. Fall, R. Jones, S. Öberg, and P. R. Briddon, Calculated properties of point defects in Be-doped GaN, Phys. Rev. B **67**, 205206 (2003).

[24] S. Lany and A. Zunger, Dual nature of acceptors in GaN and ZnO: The curious case of the shallow Mg_{Ga} deep state, Appl. Phys. Lett. **96**, 142114 (2010).

[25] J. L. Lyons, A. Janotti, and C. G. Van de Walle, Impact of Group-II acceptors on the electrical and optical properties of GaN, Jpn. J. Appl. Phys. **52**, 08JJ04 (2013).

[26] J. Buckeridge, C. R. A. Catlow, D. O. Scanlon, T. W. Keal, P. Sherwood, M. Miskufova, A. Walsh, S. M. Woodley, and A. A. Sokol, Determination of the Nitrogen Vacancy As a Shallow Compensating Center in GaN Doped with Divalent Metals, Phys. Rev. Lett. **114**, 016405 (2015).

[27] G. Miceli and A. Pasquarello, Migration of Mg and other interstitial metal dopants in GaN, Phys. Status Solidi RRL **11**, 1700081 (2017).

[28] X. Cai, J. Yang, P. Zhang, and S. H. Wei, Origin of Deep Be Acceptor Levels in Nitride Semiconductors: The Roles of Chemical and Strain Effects, Phys. Rev. Appl. **11**, 034019 (2019).

[29] S. Jin, X. Li, W. Yang, Y. Zhao, L. Bian, and S. Lu, Electrical and optical properties of beryllium deep acceptors in GaN, J. Electronic Mater. **49**, 7472 (2020).

[30] D. O. Demchenko, M. Vorobiov, O. Andrieiev, T. H. Myers, and M. A. Reshchikov, Shallow and Deep States of Beryllium Acceptor in GaN: Why Photoluminescence Experiments Do Not Reveal Small Polarons for Defects in Semiconductors, Phys. Rev. Lett. **126**, 027401 (2021).

[31] D. O. Demchenko and M. A. Reshchikov, Passivation of the beryllium acceptor in GaN and a possible route for *p*-type doping, Appl. Phys. Lett. **118**, 142103 (2021).

[32] Y. C. Tsai and C. Bayram, Mitigate self-compensation with high crystal symmetry: A first-principles study of formation and activation of impurities in GaN, Comput. Mater. Sci. **190**, 110283 (2021).

[33] F. Tuomisto, V. Prozheeva, I. Makkonen, T. H. Myers, M. Bockowski, and H. Teisseyre, Amphoteric Be in GaN: Experimental Evidence for Switching between Substitutional and Interstitial Lattice Sites, Phys. Rev. Lett. **119**, 196404 (2017).

[34] H. Hofsäss and G. Lindner, Emission channeling and blocking, Phys. Rep. **201**, 121 (1991).

[35] U. Wahl, Advances in electron emission channeling measurements in semiconductors, Hyperfine Interact. **129**, 349 (2000).

[36] U. Wahl, J. G. Correia, A. Czermak, S. Jahn, P. Jalocha, J. Marques, A. Rudge, F. Schopper, J. C. Soares, and A. Vantomme, Position-sensitive Si pad detectors for electron emission channeling experiments, Nucl. Instrum. Methods Phys. Res., Sect. A **524**, 245 (2004).

[37] L. M. C. Pereira, A. Vantomme, and U. Wahl, Characterizing defects with ion beam analysis and channeling techniques, in

Characterisation and Control of Defects in Semiconductors, edited by F. Tuomisto (Institution of Engineering and Technology, Stevenage, UK, 2019), Chap. 11, pp. 501–563.

[38] See Supplemental Material at http://link.aps.org/supplemental/10.1103/PhysRevB.105.184112 for details on GaN samples, the position of Bei, many-beam simulations, theoretical patterns for various sites, experimental patterns from nid-GaN samples, and background correction factors.

[39] E. David-Bosne, U. Wahl, J. G. Correia, T. A. L. Lima, A. Vantomme, and L. M. C. Pereira, A generalized fitting tool for analysis of two-dimensional channeling patterns, Nucl. Instrum. Methods Phys. Res., Sect. B **462**, 102 (2020).

[40] R. Catherall, W. Andreazza, M. Breitenfeldt, A. Dorsival, G. J. Focker, T. P. Gharsa, T. J. Giles, J. L. Grenard, F. Locci, P. Martins, S. Marzari, J. Schipper, A. Shornikov, and T. Stora, The ISOLDE facility, J. Phys. G **44**, 094002 (2017).

[41] V. Fedosseev, K. Chrysalidis, T. Day Goodacre, B. Marsh, S. Rothe, C. Seiffert, and K. Wendt, Ion beam production and study of radioactive isotopes with the laser ion source at ISOLDE, J. Phys. G **44**, 084006 (2017).

[42] F. Karouta, M. J. Kappers, M. C. J. C. M. Krämer, and B. Jacobs, Enhancement of p-GaN Conductivity Using PECVD SiO_x, Electrochem. Solid-State Lett. **8**, G170 (2005).

[43] M. R. Silva, U. Wahl, J. G. Correia, L. M. Amorim, and L. M. C. Pereira, A versatile apparatus for on-line emission channeling experiments, Rev. Sci. Instrum. **84**, 073506 (2013).

[44] J. F. Ziegler, M. D. Ziegler, and J. P. Biersack, SRIM - The stopping and range of ions in matter (2010), Nucl. Instrum. Methods Phys. Res., Sect. B **268**, 1818 (2010).

[45] M. Maietta, G. Vandoni, M. Ady, A. Dorsival, R. Kersevan, and A. Gottberg, Propagation of radioactive contaminants along the Isolde beamline, in *Proceedings of IPAC'15, the 6th International Particle Accelerator Conference*, edited by S. Henderson, T. Satogata, and V. R. W. Schaa (JACoW, Geneva, Switzerland, 2015), pp. 3115–3118.

[46] K. Saarinen, T. Laine, S. Kuisma, J. Nissilä, P. Hautojärvi, L. Dobrzynski, J. M. Baranowski, K. Pakula, R. Stepniewski, M. Wojdak, A. Wysmolek, T. Suski, M. Leszczynski, I. Grzegory, and S. Porowski, Observation of Native Ga Vacancies in GaN by Positron Annihilation, Phys. Rev. Lett. **79**, 3030 (1997).

[47] K. Saarinen, P. Seppälä, J. Oila, P. Hautojärvi, C. Corbel, O. Briot, and R. L. Aulombard, Gallium vacancies and the growth stoichiometry of GaN studied by positron annihilation spectroscopy, Appl. Phys. Lett. **73**, 3253 (1998).

[48] J. Oila, V. Ranki, J. Kivioja, K. Saarinen, and P. Hautojärvi, J. Likonen, J. M. Baranowski, and K. Pakula, T. Suski, M. Leszczynski, and I. Grzegory, Influence of dopants and substrate material on the formation of Ga vacancies in epitaxial GaN layers, Phys. Rev. B **63**, 045205 (2001).

[49] A. Uedono, S. Takashima, M. Edo, K. Ueno, H. Matsuyama, W. Egger, T. Koschine, C. Hugenschmidt, M. Dickmann, K. Kojima, S. F. Chichibu, and S. Ishibashi, Carrier trapping by vacancy-type defects in Mg-implanted GaN studied using monoenergetic positron beams, Phys. Status Solidi B **255**, 1700521 (2018).

[50] U. Wahl, E. David-Bosne, L. M. Amorim, A. R. G. Costa, B. De Vries, J. G. Correia, M. R. da Silva, L. M. C. Pereira, and A. Vantomme, Lattice sites of implanted Na in GaN and AlN in comparison to other light alkalis and alkaline earths, J. Appl. Phys. **128**, 045703 (2020).

[51] U. Wahl, J. G. Correia, A. R. G. Costa, T. A. L. Lima, G. Magchiels, M. R. da Silva, S. M. Tunhuma, R. Villarreal, M. J. Kappers, A. Vantomme, and L. M. C. Pereira (unpublished).